The cosmic-ray positron excess and its imprint in the Galactic gamma-ray sky

M. Rocamora,[a] Y. Ascasibar [ID],[b,c] M.A. Sánchez-Conde [ID],[b,d] M. Wechakama [ID][e,f] and P. de la Torre Luque [ID][b,d,g]

[a]*Universität Innsbruck, Institut für Astro- und Teilchenphysik,*
Technikerstr. 25/8, 6020 Innsbruck, Austria

[b]*Departamento de Física Teórica, M-15, Universidad Autónoma de Madrid, E-28049 Madrid, Spain*

[c]*Centro de Investigación Avanzada en Física Fundamental (CIAFF-UAM), Madrid, Spain*

[d]*Instituto de Física Teórica UAM-CSIC, Universidad Autónoma de Madrid,*
C/ Nicolás Cabrera, 13-15, 28049 Madrid, Spain

[e]*Kasetsart University, 50 Ngamwongwan Rd., Lat Yao, Chatuchak, Bangkok 10900, Thailand*

[f]*National Astronomical Research Institute of Thailand,*
Don Kaeo, MaeRim, Chiang Mai 50180, Thailand

[g]*Stockholm University and The Oskar Klein Center for Cosmoparticle Physics,*
Alba Nova 10691 Stockholm, Sweden

E-mail: manuel.rocamora@uibk.ac.at, yago.ascasibar@uam.es, miguel.sanchezconde@uam.es, maneenate.w@ac.th, pedro.delatorre@uam.es

ABSTRACT: We study the origin of the positron excess observed in the local cosmic-ray spectrum at high energies, and relate it to the cosmic rays and gamma-ray emission across the entire Galaxy. In particular, we explore the hypothesis of a single, dominant source accountable for primary electron-positron pairs. Since we are agnostic about the physical nature of the underlying source population, we consider four models that are representative of young pulsars, old stars (as a tracer of millisecond pulsars), and annihilating dark matter particles. In the dark matter hypothesis, we consider both a cored and a cuspy model for the halo in the Milky Way. Then, we compare the associated gamma-ray sky maps with *Fermi*-LAT data. We find that the emission arising from pulsar wind nebulae is fairly concentrated near the mid plane, and therefore additional cosmic-ray sources must be invoked to explain the emission at the center of the Galaxy. If the local positron excess were mainly due to millisecond pulsars, inverse Compton scattering by the particles injected would naturally account for a non-negligible fraction of the central gamma-ray emission. The same process would lead to a tension for a standard NFW dark matter profile, exceeding the gamma-ray data by almost a factor of 2 in some regions of the Galaxy. Although the results for an isothermal, cored profile are in agreement with these data, the cross section needed in both cases is around 2 orders of magnitude above the thermal cross-section, disfavouring the dark matter interpretation.

https://doi.org/10.1088/1475-7516/2024/07/014

JCAP07(2024)014

Contents

1 Introduction

After more than a century of intense research, the origin of cosmic-ray (CR) positrons is still not fully understood. It is now widely accepted that most Galactic CRs are accelerated in supernova remnants [1]. Secondary positrons, produced by the collision of the relativistic protons with the surrounding interstellar matter, are able to account for the observed spectrum of Galactic positrons up to $\sim 10\,\text{GeV}$ [2]. However, observational evidence strongly suggests the presence of an additional Galactic source yet to be identified. Positrons lose their energy through a variety of processes, until they eventually annihilate with electrons in the interstellar medium. The morphology of the $511\,\text{keV}$ line (see, e.g., [3], and references therein) exhibits an unexpected excess near the Galactic centre. This excess is more consistent with the morphology of the Milky Way bulge than with the distribution of the supernova remnants, which traces more closely the Galactic disk (see, e.g., refs. [4, 5]). Moreover, the PAMELA experiment measured in 2008 the energy spectrum of different CR species between 1 and $100\,\text{GeV}$ [6]. While the results obtained for the positron abundance at energies below $10\,\text{GeV}$ were fairly compatible with the predictions of the theoretical models based on a secondary origin (i.e. from primary proton spallation), it became clear that extra sources of primary positrons were necessary to explain the observed positron fraction above that energy. These results were later confirmed by other experiments, such as AMS-02 [7] and the *Fermi* Large Area Telescope (*Fermi* LAT) [8], and a secondary origin of the high-energy positrons has been confidently ruled out by comparison with the antiproton spectrum [9]. The nature of the required source of primary positrons is nonetheless heavily debated, and several theories have been proposed. Currently, the most favoured candidates are Pulsar Wind Nebulae (PWN) [10–16] and the annihilation of Dark Matter (DM) particles within the Milky Way halo [17–20]. These two sources have been extensively studied, focusing on reproducing the local positron spectrum without discussing the implications beyond the Solar neighbourhood in detail.

A complementary view of the CR population arises from the observation of their gamma-ray radiation. The measurements conducted by *Fermi* LAT have significantly enhanced our comprehension of the high-energy sky in the past 15 years. However, there are some features of the diffuse emission whose origin is still an open question. The GeV excess around the centre of the Milky Way, discovered in 2009 [21–33], was soon reported to be consistent with DM annihilation on the basis of both its spectrum and its spherically-symmetric spatial morphology. Subsequent studies proposed a population of re-accelerated MilliSecond Pulsars (MSPs) as an alternative explanation [34, 35]. These sources would also inject positrons throughout the whole Galaxy, and therefore they have also been considered as possible contributors to the local positron excess [36, 37].

Many previous studies of the gamma-ray sky describe it in terms of spatial and spectral templates that trace different components [e.g. 38–40], while more physically-motivated models of the injection and propagation of CR do not specifically address the positron excess problem [41–45]. In this work, we test whether the contribution of DM, PWN or MSP could account for both the high-energy positrons observed in the Solar neighbourhood, as well as the gamma-ray emission from the whole Galaxy. The aim of this work is not to derive constraints or upper limits to the different possible models here considered, but to explore the possibility, as a proof of concept, of building a self-consistent model that is able to explain simultaneously the origin of all CR species, including positrons, as well as 100% of the gamma-ray emission. This is, of course, a challenging endeavour, given the large number of parameters involved, and to our knowledge there is as yet no broad consensus on its feasibility, nor the minimum number of components that are required to account for all the known 'excesses' in the multi-messenger data. The CR propagation model used in this work is fully described in section 2. We follow a model-agnostic approach, where the positron energy spectrum is set by comparing to the local measurements [19, 46–50], and the spatial distribution depends on the nature of the sources tested in this work. The adopted injection spectra are discussed in section 3. Since we are not relying on any specific physical model, our conclusions will be valid for any source population that a) explains the local positron excess b) its spatial distribution is akin to those studied in the present work (i.e. young/old stars, and a cored/cuspy dark matter halo). Section 4 focuses on the comparison between the predicted gamma-ray emission and the all-sky maps from the *Fermi*-LAT Collaboration.[1] The implications for the DM, PWN, and MSP scenarios are discussed in section 5, and our main conclusions are briefly summarised in section 6.

2 Cosmic-ray propagation model

We assume that the injection and propagation of cosmic rays in the Milky Way is governed by the stationary advection-diffusion equation [51, 52]:

$$
-\overrightarrow{\nabla} \cdot \left(D \overrightarrow{\nabla} \Psi_i + \overrightarrow{v}_w \Psi_i \right) + \frac{\partial}{\partial p} \left[p^2 D_{pp} \frac{\partial}{\partial p} \left(\frac{\Psi_i}{p^2} \right) \right] - \frac{\partial}{\partial p} \left[\dot{p} \Psi_i - \frac{p}{3} \left(\overrightarrow{\nabla} \cdot \overrightarrow{v}_w \right) \Psi_i \right]
$$
$$
= Q_i + \sum_{i<j} \left(c \, \beta \, n_{\text{gas}} \, \sigma_{j \to i} + \frac{1}{\gamma \tau_{j \to i}} \right) \Psi_j - \left(c \, \beta \, n_{\text{gas}} \, \sigma_i + \frac{1}{\gamma \tau_i} \right) \Psi_i \quad (2.1)
$$

---

[1]*Fermi*-LAT data repository: https://fermi.gsfc.nasa.gov/ssc/data/access/.

where Ψ_i denotes the spectrum (number of particles per unit volume per unit momentum) of CR species i, D is the spatial diffusion coefficient, and v_w is the effective wind velocity in the Galaxy; p denotes the momentum of the particles, and D_{pp} refers to diffusion in momentum space; the $\dot{p}$ and the following term represent the momentum and the adiabatic losses, respectively; Q_i is the source term (injection spectrum per unit time); c represents the speed of light, β and γ are the velocity and Lorentz factor, respectively, n_{gas} is the number density of the interstellar gas particles, $\sigma_{j\to i}$ is the spallation cross-section of species j into i by collision with gas particles, $\tau_{j\to i}$ represents the lifetime for spontaneous decay, $\sigma_i \equiv \sum_{j<i} \sigma_{i\to j}$, and $1/\tau_i \equiv \sum_{j<i} 1/\tau_{i\to j}$.

This equation is solved numerically using the DRAGON CR propagation code[2] [53] on a uniform spatial and energy grid. We use a simulation box given by a 2-dimensional cylindrical spatial grid with radial coordinate $R \in [0, 12]$ kpc and 121 grid points, and vertical coordinate $z \in [-18, 18]$ kpc with 361 grid points, i.e. a uniform spatial resolution of 0.1 kpc in both dimensions, and study energies in the range $E_k \in [10\,\text{MeV}, 100\,\text{TeV}]$, using 90 logarithmically spaced energy bins. Note that these radial and vertical scales correspond to the size of the simulation box in each dimension, not to the physical scales of the Galactic halo, which will be discussed in section 2.2. We verified that the adopted resolution and box size ensure numerical convergence within a few percent. In the radial direction, our setup is identical to [15]; in the vertical direction, we increase the box height in order to improve our modelling of the gamma-ray emission at high latitudes.

2.1 Source terms

Following previous works [e.g 15, 54, 55], we use a broken power-law

$$Q_{\text{SNR}}(R, z, E) = Q_0 \, S(R, z) \begin{cases} \left(\dfrac{E}{E_1}\right)^{\alpha_0} & \Longleftrightarrow & E < E_1 \\[2mm] \left(\dfrac{E}{E_1}\right)^{\alpha_1} & \Longleftrightarrow & E_1 < E < E_2 \\[2mm] \left(\dfrac{E_2}{E_1}\right)^{\alpha_1} \left(\dfrac{E}{E_2}\right)^{\alpha_2} & \Longleftrightarrow & E > E_2 \end{cases} \qquad (2.2)$$

to model the injection of protons and heavier nuclei by SuperNova Remnant (SNR) shocks. For electrons, an additional exponential cut-off $e^{-E/E_{\text{cut}}}$ is included at high energies. The overall normalisation constant $Q_0 \equiv Q(R_\odot, 0, E_0)$, i.e. the injection rate at the Solar location ($R = R_\odot = 8.3\,\text{kpc}$, $z = 0$) at an arbitrary reference energy $E_0 \equiv 1\,\text{GeV}$, as well as the logarithmic slopes α_0, α_1, α_2, and the break energies E_1 and E_2, are free parameters to be determined independently for each particle species, whose values are set to reproduce the local CR data.

In order to explain the observed positron spectrum, it is necessary to postulate a new source of primary electron-positron pairs, which we refer to as the 'extra component'. To model its injection spectrum as a function of energy, we use a single power-law with an exponential cut-off [56]:

$$Q_{\text{extra}}(R, z, E) = Q_0 \, S(R, z) \left(\frac{E}{E_0}\right)^{\alpha} e^{-E/E_{\text{cut}}}, \qquad (2.3)$$

---

[2]https://github.com/cosmicrays/DRAGON2-Beta_version.

where the normalisation Q_0, the logarithmic slope α and the cut-off energy $E_{\rm cut}$ are varied as free parameters, while $E_0 \equiv 1\,{\rm GeV}$ merely denotes, once again, the reference energy adopted to express Q_0. Although every single pulsar (PWN or MSP) may feature a unique injection spectrum, this simple analytical form provides a fair approximation to describe the sum over the whole population of individual sources. In the context of DM annihilation, instead of assuming a specific particle physics model (e.g. mass and branching ratios for the different annihilation channels), we here remain completely agnostic about the precise nature of the DM particles, and simply use this phenomenological injection spectrum under the assumption that their annihilation is the main physical mechanism responsible for the local positron excess. The spectrum of particles produced by DM annihilation could feature sharp cut-offs. However, we will limit ourselves to study simple exponential ones.

Regarding the spatial distribution $S(R, z)$, we adopt a Ferriere [57] profile:

$$
\begin{aligned}
S_{\rm SNR}(R, z) = {} & 7.3 \exp\left(-\frac{R-R_\odot}{4.5} - \frac{|z|}{0.325}\right) + \left[0.79 \exp\left(-\left(\frac{z}{0.212}\right)^2\right) + 0.21 \exp\left(-\left(\frac{z}{0.636}\right)^2\right)\right] \\
& \times \begin{cases} 177.5 \exp\left(-\dfrac{(R-3.7)^2}{2.1^2}\right) & \Longleftrightarrow \quad R < 3.7 \\[2ex] 50.0 \exp\left(-\dfrac{R^2-R_\odot^2}{6.8^2}\right) & \Longleftrightarrow \quad R > 3.7 \end{cases}
\end{aligned}
\tag{2.4}
$$

to describe the distribution of Galactic SNR.

For PWN, we adopt a Lorimer profile [58]:

$$
S_{\rm PWN}(R, z) = \left(\frac{R}{R_\odot}\right)^{1.9} \exp\left(-5.0\,\frac{R-R_\odot}{R_\odot} - \frac{|z|}{0.2}\right)
\tag{2.5}
$$

to describe the distribution of pulsars in the Milky Way.

The only MSPs capable of accelerating particles above $10\,{\rm GeV}$ are those inside compact binary systems [36]. A limited number of these systems have been discovered in the Galaxy so far, and so their distribution is poorly known. Therefore, we decide to use a McMillan profile in this case: [59]

$$
\begin{aligned}
S_{\rm MSP}(R, z) = {} & \frac{98.4}{(1 + R'/0.075)^{1.8}} \exp\left(-\frac{R^2 + (z/0.5)^2}{2.1^2}\right) + \frac{896}{2 \cdot 300} \exp\left(-\frac{|z|}{0.3} - \frac{R}{2.5}\right) \\
& + \frac{183}{2 \cdot 900} \exp\left(-\frac{|z|}{0.9} - \frac{R}{3.02}\right),
\end{aligned}
\tag{2.6}
$$

where $R' = \sqrt{R^2 + (z/0.5)^2}$. This function describes the overall distribution of stars within the Galaxy, as a first order approximation of the location of MSPs.

Finally, the annihilation rate of DM particles in the Milky Way halo is proportional to the square of the DM density, whose behaviour in the innermost regions is still debated (the so-called "cusp-core" problem [60–63]). In this work, we will study two distributions: the one proposed in ref. [64] following the results found in cosmological simulations (the so-called 'NFW' profile), and an isothermal (ISO) profile [65]. These are representative of both cuspy and cored DM distributions, respectively. The difference between cuspy and cored profiles
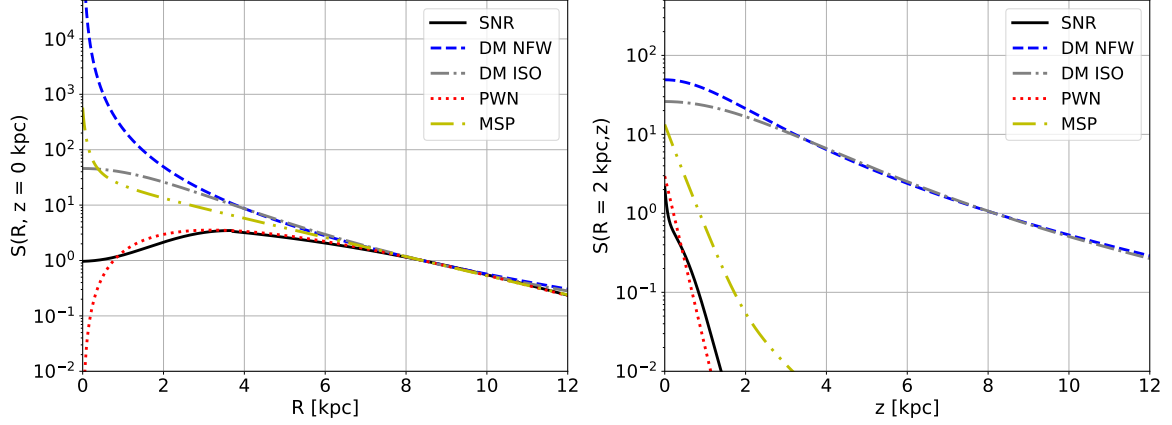
Figure 1. Particle injection profiles as a function of Galactocentric radius at z = 0 (left) and in terms of height from the Galactic plane at R = 2 kpc (right).

lie at the center of the DM halo, while the former has a pronounced peak, the latter is flat. The NFW and ISO profiles squared read as follows:

$$S_{\mathrm{NFW}}(r) = \frac{1}{(r/r_s)^2(1 + r/r_s)^4} \tag{2.7}$$

$$S_{\mathrm{ISO}}(r) = \frac{1}{(1 + (r/r_{\mathrm{iso}})^2)^2} \tag{2.8}$$

where $r \equiv \sqrt{R^2 + z^2}$ is the spherical radial coordinate, whereas $r_s = 20\,\mathrm{kpc}$ [66] and $r_{\mathrm{iso}} = 3.5\,\mathrm{kpc}$ [67] denote the scale radius of the DM halo in each profile.

The spatial distributions of the different CR sources are shown in figure 1. The density of SNR and PWN is quite uniform across the inner Milky Way disk, peaking a few kpc away from the Galactic centre, whereas MSP and DM are much more concentrated, tracing the morphology of the stellar bulge and of the DM halo, respectively. Therefore, they are expected to yield very different predictions about the CR and gamma-ray spectra in the innermost regions of the Galaxy, once they match the Solar neighbourhood measurements. As one can see on the right panel, the DM profiles (both NFW and ISO) extend up to much higher latitudes that the exponentially decaying injection profiles of the pulsar scenario (PWN and MSP).

2.2 Propagation parameters

The energy losses considered in this work are pion production, Coulomb scattering, ionization, bremsstrahlung, inverse Compton scattering (including the Klein Nishina regime) and synchrotron radiation, all of them included by default in DRAGON [see appendix C.10 in 53]. For the magnetic field, we use the model of [68], adding a turbulent component to match the observed local value of $\sim 6\ \mu G$ [57]. We assume the shape of the turbulent component as [69, 70]

$$B_{\mathrm{turb}} = B_{0,\mathrm{turb}}\ \exp\left(-\frac{R - R_\odot}{r_0}\right)\exp(-|z|/z_t), \tag{2.9}$$

where z_t is the scale height of the Galactic magnetic field, not to be confused with the size of the simulation box, $B_{0,\mathrm{turb}} = 5.5\ \mu G$, $r_0 = 8.5\,\mathrm{kpc}$.

R_{max} [kpc]	z_{max} [kpc]	D_0 [cm^2/s]	δ	v_A [km/s]	z_t [kpc]	$\langle \phi_{mod} \rangle$	k_σ
12	18	1.1×10^{28}	0.68	13.0	4	0.58	1.5

Table 1. Box size and propagation parameters of our model, manually set by comparison with local measurements of the CR spectra. D_0 is specified at a referenge rigidity of $1\,\mathrm{GV}$.

In order to ensure self-consistency, we adopt the same gas density model as the HERMES[3] code [71], that we will later use to compute the gamma-ray emission. This model is composed of 11 Galactocentric rings of gas column density derived from the HI4PI survey [72] and the CfA survey [73] for atomic and molecular gas, respectively. For the molecular gas, we use a constant X_{CO} factor of $1.9 \times 10^{20}\,\mathrm{cm}^{-2}\,\mathrm{K}^{-1}/(\mathrm{km}\ \mathrm{s}^{-1})$ [74].

We make use of the DRAGON default cross sections, described in [75], to calculate the nuclear secondaries, and the Kamae cross section [76] to calculate the secondary electrons and positrons.

For the diffusion coefficient, we assume that it follows a single power-law in particle rigidity ρ, and it increases exponentially with the height $|z|$ over the Galactic mid-plane, driven by the decay of the magnetic field [55]:

$$D(\rho, z) = D_0 \left(\frac{\rho}{\rho_0} \right)^\delta \exp(|z|/z_t), \tag{2.10}$$

with reference rigidity $\rho_0 = 1\,\mathrm{GV}$. The normalisation D_0, the logarithmic slope δ, and the characteristic scale height z_t are free parameters of the model (see table 1). This leads to a diffusion in momentum space, also known as re-acceleration, whose coefficient is given by [52]:

$$D_{pp} = \frac{4}{3\delta(4 - \delta^2)(4 - \delta)} \frac{p^2 v_A^2}{\langle D \rangle}, \tag{2.11}$$

where v_A is the Alfvén velocity and $\langle D \rangle$ is the spatial diffusion coefficient from eq. (2.10) averaged over all the directions.

3 Cosmic-ray spectra

In order to determine the free parameters in our model, we make use of 7 years of B/C, He, p, e^- and e^+ data from AMS [77], as well as H.E.S.S. measurements of the combined $e^- + e^+$ spectrum [78]. We also consider the Voyager-1 mission data [79] to investigate the effect of the Sun at low energies, that we describe by means of the Force Field approximation [80, 81] for simplicity, where the modulation potential $\langle \phi_{mod} \rangle$ is an additional free variable. This description has large uncertainties, especially at low energies, but a more detailed modelling of the Heliosphere is beyond the scope of this work.

Any physically motivated model of the Galactic CRs necessarily involves a large number of free parameters. In our case, we have six (normalisation, logarithmic slopes, and breaks) for the primary injection of each particle species (electrons, protons, Helium, Carbon, and Oxygen) by SNR, another three (normalisation, slope, and cut-off) for the extra component (be

---

[3]https://github.com/cosmicrays/hermes.

it PWN, MSP, or DM), and five more associated to particle propagation. Our prior knowledge of their true values is, at best, uncertain, and they are strongly degenerate. Exploring in a proper way such a vast parameter space with $(6 \times 5 + 3 \times 3 + 5) = 44$ dimensions and evaluating the uncertainties associated to the fits (with, e.g. a Markov-Chain Monte Carlo approach) is extremely challenging from a computational point of view. Moreover, it would only provide a rigorous quantification of the statistical uncertainties, yet neglecting the significant systematic biases incurred by our choice of astrophysical parameters associated to the Milky Way, such as the gas density, magnetic field, radiation field, and spatial distribution $S_i(R, z)$ of the different sources.

For these reasons, we do not attempt to find the model that best fits the observational data. Instead, this work aims to investigate whether it is possible to explain all the available CR and gamma-ray measurements in terms of two source populations, namely SNR and the 'extra component', and whether PWN, MSP, or DM would be viable candidates for the latter. To that end, we adjust manually the parameter values until we find a $\sim 1\sigma$ agreement with the data.

3.1 Procedure and baseline model

We first set the CR propagation parameters and the primary injection of nuclei in the baseline SNR model. We reproduce the local data on hadronic species by exploring combinations of the propagation parameters. Then, we do the same for the injection spectrum of primary electrons by SNR, constrained by the corresponding spectra at very low and high energies. Finally, we investigate and discuss the injection of additional primary electrons and positrons in our four 'extra component' scenarios. During this procedure, we could not explain the low energy tail of the positron spectrum by only varying the propagation parameters of the model, with a flux prediction always around a factor of 2 below the data. Because of that, and given the uncertainties in the modelling of the local flux of secondary positrons [82–85], we apply a fudge multiplicative factor, k_σ to the cross section. This parameter, constant with the energy, simply scales the cross section. It is included in our tuning procedure and allows us to reproduce the low energy positrons.

In the baseline model, all CRs are injected by sources following the distribution of supernova remnants. The proposed values of the propagation parameters are quoted in table 1, whereas the injection of each particle species is specified in table 2. The predictions for the CR flux, J(E), of this model are compared in figure 2 with the available observational measurements. Although some discrepancies are still present, one may conclude that, in general, all the hadronic spectra (H, He, B/C, and O) are fairly well reproduced, taking into account current systematic uncertainties.

The most notable deviation corresponds to the Boron-to-Carbon ratio, both at low and high energies. We find that above $\sim 100 \,\mathrm{GeV}$ this ratio starts to deviate more significantly from the data. This has been explained in the literature as a change in the diffusion regime [48, 86]. However, we do not model such a feature because it introduces more degenerate free parameters in our procedure. In our case, where such a break is not modelled, we note that it is necessary to introduce a similar feature in the injection spectra [87] at the energy scale we label as E_2. For Oxygen, Carbon and Helium, we adopt $E_2 = 100 \,\mathrm{GeV}$, and a somewhat larger value

Species	Q_0 [GeV^{-1} m^{-3} Myr^{-1}]	$-\alpha_0$	E_1 [GeV]	$-\alpha_1$	E_2 [GeV]	$-\alpha_2$	E_{cut} [GeV]
O	1.72×10^{-7}	2.00	7.0	2.25	100	2.03	—
C	1.33×10^{-7}	2.00	7.0	2.23	100	2.03	—
He	3.62×10^{-6}	2.00	7.0	2.21	100	2.05	—
H	2.17×10^{-5}	1.80	7.0	2.21	335	2.05	—
e^-	7.91×10^{-7}	2.00	8.0	2.70	60	2.46	2×10^4

Table 2. Injection parameters of the baseline SNR model. The normalization of the injection spectra, Q_0, is given at $E_0 = 1\,\text{GeV}$; E_i is the energy of the different breaks; E_{cut} denotes the cut-off energy, and α_i are the logarithmic slopes of the injection spectra.

is required in order to accurately reproduce the observed proton spectrum, that displays a significant feature at $E_2 \sim 300\,\text{GeV}$. In the intermediate energy range $E_1 < E < E_2$, our logarithmic slope α_1 is slightly steeper than the canonical value $\alpha \sim -2$.

In what concerns the propagation parameters, that are mainly determined by the secondary species B and e$^+$, we observe that the resulting diffusion index $\delta = 0.68$ is a bit above the values typically obtained from the quasi-linear theory of diffusion, which predicts an index ranging between $1/3$ and $1/2$, depending on the turbulence model [88]. Nevertheless, recent studies have also given results consistent with ours [16, 48, 89, 90]. The Alfvén velocity varies a lot among the different studies, but it is typically lower than $40\,\text{km/s}$ [15, 44, 46, 49, 50], which is consistent with our result of $13\,\text{km/s}$. A height $z_t = 4\,\text{kpc}$ has been typically used and is in agreement with current observations of the ^{10}Be isotope [48, 49]. The modulation potential is also in good agreement with the results of ground-based measurements [80, 81]. Its effect is shown e.g. in the proton spectrum in figure 2, where the solid and dash-dotted lines show the spectrum with and without the solar modulation, respectively. The same modulation value of $\langle \phi_{\text{mod}} \rangle = 0.58$ is used for every particle. Its uncertainty of ± 0.1, according to [15, 80, 81], is shown as a gray band in the protons and leptons spectra. The impact of the modulation is stronger in the positrons, since the same modulation values result in a wider uncertainty band. Finally, we consider that our fudge multiplicative factor for the positron production cross-section, k_σ, is compatible with the present uncertainties [82].

3.2 Extra component

Regarding the extra component, we look for the normalisation, injection index and cut-off energy that is consistent with the positron and electron spectra observed at the Solar neighbourhood for each one of the adopted source morphologies (PWN, MSP, DM NFW and DM ISO). The numerical results are given in table 3, and figure 3 shows the comparison between the model predictions and the experimental data.

The injection index and cut-off in the young pulsar scenario are 1.55 and $750\,\text{GeV}$, respectively, which is in good agreement with the expected PWNe index injection from gamma-ray observations, between 1.2–2.2 [13, 91]. In the case of the MSP, our result of 1.5 also fits well in the typical range (1.5–2.5) used for MSPs [92, 93]. The two considered
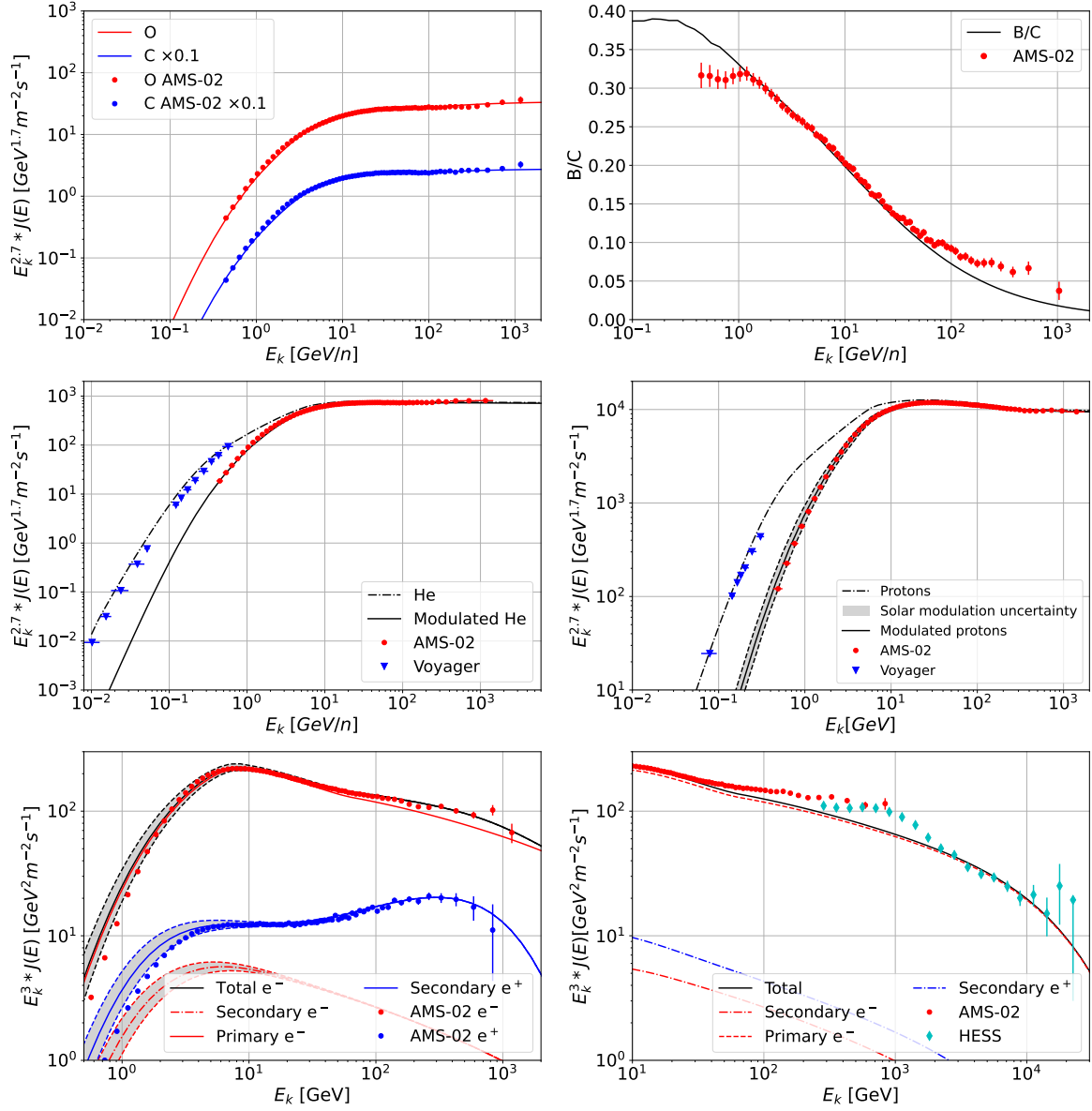
Figure 2. CR spectrum of our model at Earth for Oxygen and Carbon, the latter is multiplied by 0.1 for a better visibility (top left); Boron-to-Carbon ratio (top right); Helium (middle left); protons (middle right); electrons and positrons at low energies (bottom left); and all-leptons at high energies (bottom right), compared to data from either AMS-02 [77], Voyager [79], or HESS [78]. The nuclei fluxes are multiplied by $E^{2.7}$, while the CR leptons by E^3. For Helium and protons, we show the effect of the solar modulation by showing AMS data (red) and Voyager data (blue). For the low-energy leptons, the red and blue colors stand for e^- and e^+, respectively. The dashed lines and grey bands show the solar modulation uncertainty.

Model	Q_0 $[\mathrm{GeV}^{-1}\,\mathrm{m}^{-3}\,\mathrm{Myr}^{-1}]$	$-\alpha$	E_{cut} [GeV]
DM NFW	1.22×10^{-10}	1.30	900
DM ISO	1.22×10^{-10}	1.30	900
PWN	3.97×10^{-9}	1.55	750
MSP	1.97×10^{-9}	1.50	800

Table 3. Injection parameters of our 'extra component' in every scenario; see eq. (2.3) for details. The parameters are described as in table 2.

DM scenarios are consistent with $\alpha = -1.30$ and $E_{\mathrm{cut}} = 900\,\mathrm{GeV}$. Although there is a large difference between both DM distributions in the innermost region of the Galaxy, at larger Galactic radii their behaviour is quite similar. Therefore, both models yield the same set of injection parameters. These values are more difficult to interpret, since we do not assume a theoretical annihilation spectrum, but the cut-off energy hints towards a DM particle mass of the order of ~ 1–$10\,\mathrm{TeV}$.

By construction, all the extra component models yield similar results in the Solar vicinity. However, large differences are expected both at the Galactic centre, as well as far from the Galactic plane, due to their different spatial distribution. Figure 4 shows the resulting CR electron (left) and positron (right) spectra at the center of the Milky Way. The effect of introducing the extra $e^- e^+$ pairs according to our four prescriptions is clearly noticeable. While the MSP and both DM scenarios produce a significant boost in the electron and positron content over a broad energy range, PWN represent a minor correction with respect to the baseline model accounting for SNR injection alone.

4 Gamma rays

Having obtained a description of the distribution of CRs within the Galaxy, we now proceed to compute their associated gamma-ray emission. To do this, we make use of the HERMES[4] code [71], where we include different processes: bremsstrahlung and Inverse Compton Scattering (ICS), coming from leptons, and π^0 decay, from protons and helium. In addition, they all include the extragalactic gamma-ray background (EGRB) described in [94, 95].

The *Fermi*-LAT data is extracted using an observation time ranging from 04-08-2008 to 31-12-2020, selecting CLEAN events from the PASS8 data and the P8R3_CLEAN_V3 version of the instrument response function. Events with zenith angle $\theta_z < 100°$ and events given when the LAT instrument was at rocking angles $\theta_r < 52°$ are removed. Our resulting skymaps are calculated using a Healpix projection parameter $nside = 256$, in order to approximately match the LAT data resolution at high energies.

Since all the scenarios share the same baseline hadronic component, they feature the same π^0 results, which can be considered as a minimal baseline model. Our CO-to-H2 conversion factor X_{CO} is lower than the values used in recent studies [e.g. 45, 96], where even
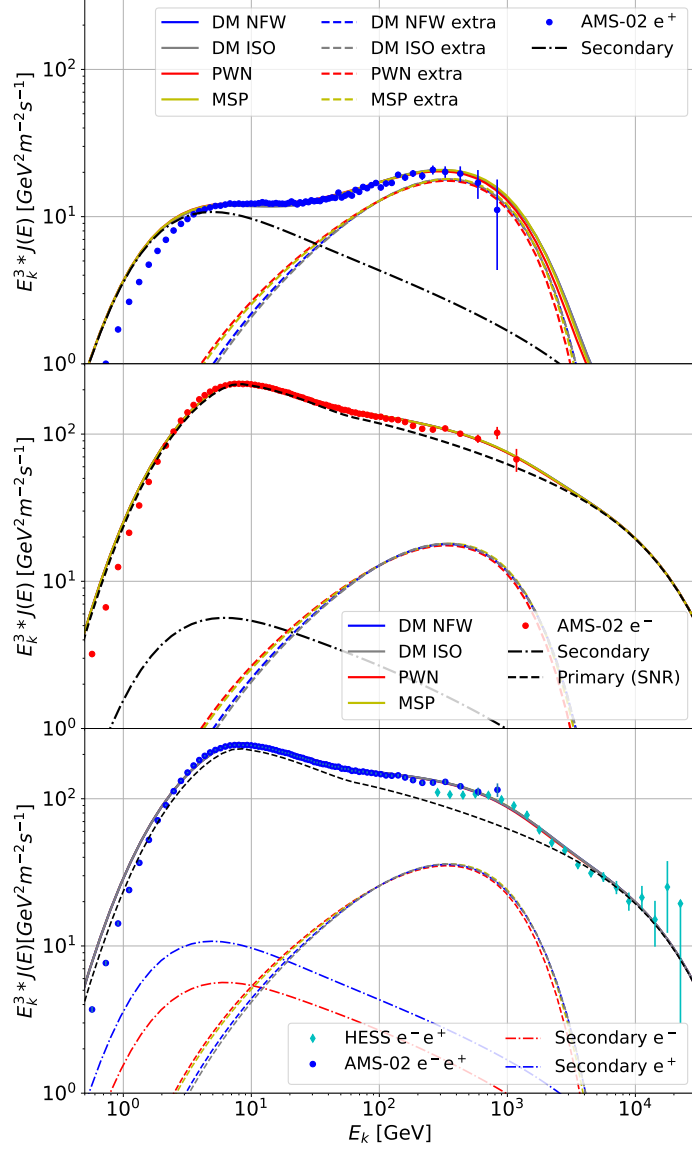
---

[4]https://github.com/cosmicrays/hermes.

Figure 3. CR positron (top), electron (middle) and all-lepton (bottom) spectra including our 'Extra' component for the three different scenarios. The dashed coloured lines show the extra component. For e⁻, the black dashed line shows the baseline primary component, while for both e⁻ and e⁺, the black dash-dotted line shows the baseline secondary component.

a variable factor depending on the Galactic radius is considered. The gamma-ray emission of the baseline SNR model can be seen in appendix A.

We show our gamma-ray maps and their residuals with respect to *Fermi*-LAT data in the energy range 10–100 GeV in the left and right columns of figure 5, respectively. We perform a 2° Gaussian smoothing in order to mitigate random statistical fluctuations. One may see the effect of point sources as compact blue circles in the residual images, but modelling these components is beyond the scope of this work.

Figure 4. CR electron (left) and positron (right) spectra at the Galactic center. Solid lines represent the sum of every component in the model.

Away from point sources, all our scenarios are able to reproduce the observations with an accuracy of the order of $\sim 30\%$, with a few exceptions. On the one hand, the PWN and MSP scenarios clearly need the introduction of another physical component (the so-called 'Fermi bubbles' [97, 98]) in order to match the data above and below the center of the Milky Way. On the other hand, DM annihilation within a cuspy (NFW) halo overshoots the observed emission by a factor of ~ 2 at intermediate latitudes ($|b| \sim 10°$). This problem may be mitigated by invoking a cored, 'DM ISO' halo. Note that at higher latitudes ($|b| \lesssim 50°$), DM annihilation would be able to account for a large fraction of the gamma-ray emission that is usually attributed to the Fermi bubbles.

We also study the spectra of our models at different regions of the sky, which are shown in figure 6. Although our approach does not aim to accurately reproduce the observational measurements, it is able to unambiguously highlight significant discrepancies. In a region of $3°$ radius (shown as a black circle in figure 5) at the center of the Galaxy (top row), the DM NFW model reproduces well the spectra, while the others are clearly below the data above $1\,\mathrm{GeV}$. On the other hand, the excess of the DM NFW scenario at energies $\gtrsim 3\,\mathrm{GeV}$ is evident, e.g., at $l = 0°$, $b = -7°$ (second row). Since our analysis does not include the prompt emission of gamma-rays, which may actually dominate over the ICS component for DM annihilation, a cuspy halo would be in tension with the gamma-ray observations if the annihilation of DM particles was responsible for a significant fraction of the high-energy positrons. A more detailed analysis, including this component, could be carried out in order to constrain the inner slope of the density profile. Based on our study, a cored DM profile such as our DM ISO model cannot be confidently ruled out. On the other hand, both PWN and MSP pulsar scenarios are perfectly compatible with the data, yet in this case one must necessarily invoke additional sources to explain the gamma-ray sky.

At variance with previous studies [41, 44], where the π^0 component dominates at every region of the Galaxy, one can readily see in figure 6 that ICS from the extra source of positrons may make a sizable contribution to the observed gamma-ray emission. For instance, at $l = 0°$, $b = -7°$ (second row) and $E = 100\,\mathrm{GeV}$, it is actually the dominant component for all the scenarios that we have considered.
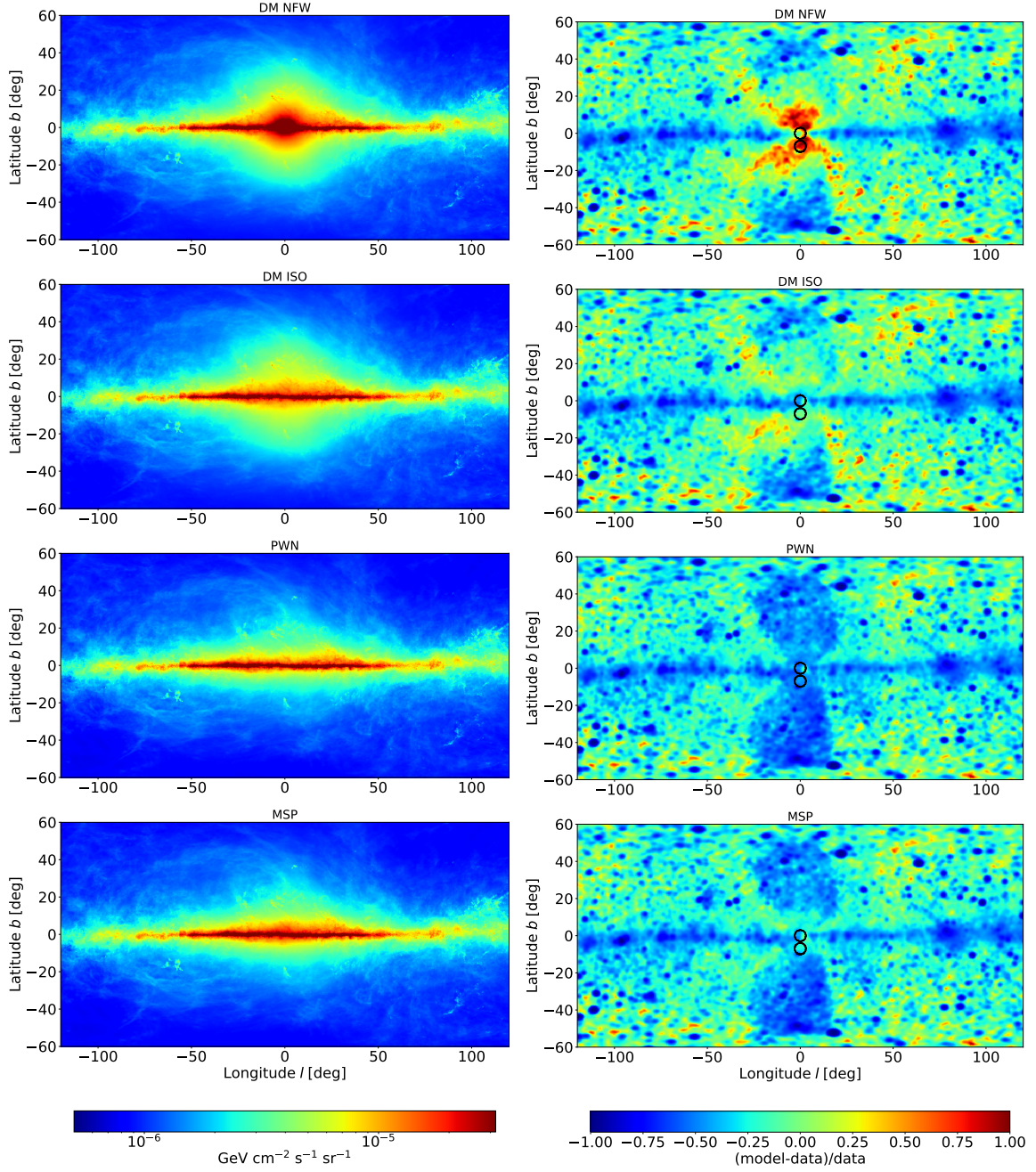
Figure 5. On the left column, total gamma-ray emission at 10–100 GeV predicted by our models (from top to bottom: DM NFW, DM ISO, PWN, and MSP). The right column shows the residuals $(model - data)/data$ with respect to the Fermi-LAT data. The maps have a Healpix projection parameter *nside* of 256, corresponding to a pixel size of $1.598 \cdot 10^{-5}$ sr. Black circles represent the 3° regions where we study the gamma-ray spectra (see figure 6).
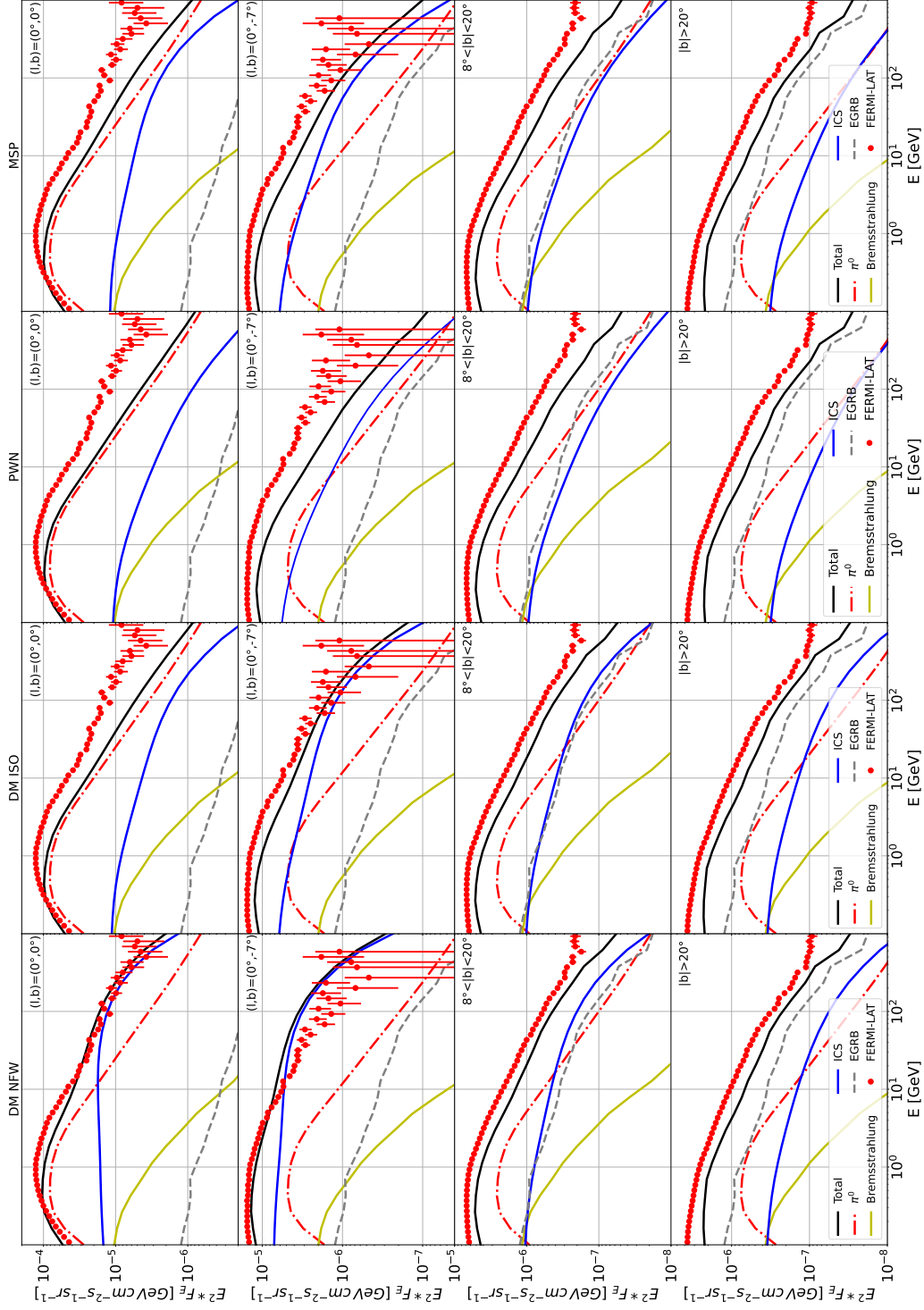
Figure 6. Gamma-ray spectra for every model (from left to right: DM NFW, DM ISO, PWN, MSP) at different sky regions (from top to bottom: Galactic center, $l = 0°$ and $b = -7°$, $8° < |b| < 20°$, $|b| > 20°$). The first two rows correspond to a circular region with a radius of $3°$ around the given point, while the latter rows cover the whole latitude range. Data points are from Fermi LAT.

5 Discussion

In principle, any of the proposed scenarios could be, at least, partially responsible for the local positron excess. Although the excess of the NFW scenario with respect to the observed emission is relatively mild (taking into account the uncertainties in the model), the missing gamma-ray components make it significant. In this regard, a cored DM (ISO) halo is compatible with the data and, therefore, favoured. Prompt emission of gamma rays should be investigated in order to derive more stringent constraints on the allowed density profiles, as already done in [17, 99] when finding non compatibility with the DM hypothesis. Given the uncertainties in the astrophysical ingredients of our model (e.g. gas density, radiation and magnetic fields across the Milky Way), we also consider that a more thorough exploration of the parameter space is necessary if we want to completely and confidently rule out the DM annihilation hypothesis [100].

On the opposite extreme, PWN are the only explanation of the local positron excess that would not have a significant gamma-ray imprint. While this is a positive trait in terms of compatibility, it implies that a more complicated model, with a combination of sources, would be needed to reproduce the observed gamma-ray emission. Thus, using the Occam's razor argument, PWN would be disfavoured if another scenario could be found that self-consistently accounted for both the local spectra and the Galactic gamma ray sky. Since our approach is quite model independent, this result applies to any explanation of the local positron excess associated to the young stellar population or simply concentrated near the Galactic plane for whatever reason. In this sense, MSP, or any other candidate source that follows the distribution of the old stellar population, provides a much better match in the central regions, and therefore these types of scenarios are certainly worth further scrutiny.

In addition to these considerations, derived from the predicted gamma-ray emission, one may take our phenomenological approach one step further and assess whether the parameters that we adopted are realistic, or at least compatible with our current knowledge. Even if the injection spectrum is tuned to match the local measurements, additional constraints may be obtained based on the energy budget available to each scenario.

To calculate the energy input, we integrate the source spectrum over the whole Galaxy. In our PWN model, the total power injected across the whole Galaxy is $(dE/dt)_{\mathrm{PWN}} = 7.2 \times 10^{37}$ erg/s. There are thousands of known young pulsars in the Milky Way, many of which are expected to host PWN and/or gamma-ray halos (see e.g. [101]). The average power per single source is thus of the order of $10^{34} - 10^{35}$ erg/s, consistent with observed spin-down luminosities. For the MSP scenario, the total injected power increases to $(dE/dt)_{\mathrm{MSP}} = 1.5 \times 10^{38}$ erg/s. Although only ~ 50 MSP have been discovered so far, it is estimated that their total number could be of the order of $(2\text{–}7) \times 10^3$ [37], yielding a similar average power per individual source. Whether this number is realistic or not depends on the physical mechanism of pair production. Our results are consistent with [14], who advocate for a 10 per cent efficiency in the conversion of spin-down luminosity in PWN. For MSP, somewhat lower values (1–10%) are reported by [37]. In such a case, the gamma-ray emission could be significantly smaller than predicted by our model.

For DM annihilation, the injected power in form of $e^- e^+$ pairs needed to reproduce the local positron excess amounts to $(dE/dt)_{\mathrm{NFW}} = 6.9 \times 10^{38}$ erg/s and $(dE/dt)_{\mathrm{ISO}} = 4.1 \times$

10^{38} erg/s. In the Solar neighbourhood, both density profiles inject a power density per unit volume $(du/dt)_{\mathrm{DM},\odot} = 6.3 \times 10^{-28}\,\mathrm{GeV/cm^3/s}$. This power density results from integrating in energy eq. (2.3) at the Solar position and is to be compared with the theoretical rate

$$\left(\frac{du}{dt}\right)_{\mathrm{DM},\odot} \approx \frac{\rho_{\mathrm{DM},\odot}^2}{m_{\mathrm{DM}}} \langle \sigma v \rangle c^2. \tag{5.1}$$

Assuming a DM particle mass of $1\,\mathrm{TeV}$ (as suggested by our results) and a local DM density $\rho_{\mathrm{DM},\odot}\,c^2 = 0.4\,\mathrm{GeV\,cm^{-3}}$ [102], we have $\langle \sigma v \rangle \approx 3.9 \times 10^{-24}\,\mathrm{cm^3/s}$ for both models, which is two orders of magnitude above the thermal annihilation cross-section, consistent with the constraints obtained by [103] for the injection of electron-positron pairs with identical initial energy $E_0 = m_{\mathrm{DM}}c^2$ and [104] for different annihilation channels.

This value may be regarded as a lower limit if we take into account that we are considering only the injected leptons, while part of the energy in a DM annihilation is actually emitted as prompt gamma-ray photons. Even in this case, the result is already in conflict with the current constraints for a cuspy DM distribution [105]. On the other hand, let us note that a particle with $m_{\mathrm{DM}}\,c^2 \sim 1$–$100\,\mathrm{GeV}$ and $\langle \sigma v \rangle \sim 3 \times 10^{-26}\,\mathrm{cm^3/s}$, with a non-negligible leptonic branching ratio (after accounting for prompt emission and other annihilation channels), might be responsible for a fraction of both the positrons in the Solar neighbourhood [106] and the Galactic gamma-rays in this energy range.

6 Conclusions

We have studied the positron excess in the local CR spectrum [6], whose origin might be related to new physics or may unveil new astrophysical mechanisms at play in the Milky Way. In addition to the secondary positron population produced in CR collisions with the Galactic gas, in this proof-of-concept work we introduced an extra source that injects symmetrically e^+e^- pairs. At variance with other studies, we do not impose any particular model, but manually adjust the injection parameters to reproduce the local measurements of the lepton spectra [77, 78]. In doing so, our conclusions are valid regardless of the actual physical mechanism(s) responsible for pair production. We considered four different scenarios for the nature of the positrons source and its distribution within the Galaxy: two for annihilation of DM particles, with squared NFW [64] and isothermal [65] DM halo density profiles, and two related to the pulsar population; PWN following a Lorimer [58] profile, and MSP (assumed to trace old stars) with a McMillan [59] profile. Since all our models reproduce, by construction, the local spectra, they yield the same positron spectrum at the Earth position, but not in other places of the Galaxy. To build these models, we only looked at local CR data and did not investigate their synchrotron emission, which depends on the magnetic field assumed. This might have an impact on the lepton distribution within the Galaxy, and therefore on the resulting ICS emission [107]. Then, we computed the gamma-ray emission associated to each scenario and compared the predicted all-sky maps with the available data from *Fermi*-LAT, to test whether the different scenarios proposed could explain the positron emission observed at Earth without being in conflict with gamma-ray data in other Galactic regions.

We first built a SNR model by comparing to CR data. Then, we added to this model the emission of ICS and bremsstrahlung coming from the electrons injected by SNRs and

the extra source matching AMS-02 positron data. Our results should be taken as a minimal model, as not every possible gamma-ray contribution is included. The $X_{\rm CO}$ value that we used for the molecular gas density is rather low, leading to a low π^0 contribution. Neither the gamma-ray point-like sources, the Fermi Bubbles nor DM prompt emission were included. Therefore, any overshoot of the data means that there are significant tensions, even with the high uncertainties in the modelling.

The predicted gamma-ray emission from our DM NFW scenario fits well the data in the center of the Galaxy. However, it has a significant tension at intermediate latitudes, where the DM ISO scenario has a better agreement with the data. In the case of PWN and MSP, they are both below the data in both regions of the Galaxy. This means that there is some freedom for the addition of the components that are missing in our minimal model. The energetics of the PWN and MSP scenarios are consistent with the observed luminosities of single sources. In the case of DM, the resulting cross-section of $3.9 \times 10^{-24}\,{\rm cm}^3/{\rm s}$ is higher than the allowed values by the current constraints [105] for a cuspy, NFW-like DM distribution. Although the constraints for a cored ISO profile should be weaker, there might also be some tension with our result, since we are not considering the prompt DM emission, i.e. the usually dominant component in the gamma-ray domain. Besides that, our results might be useful to set additional constraints even in the models where the prompt emission is suppressed [e.g. 108].

None of our single scenarios is able to simultaneously fit the positron excess and the Galactic center emission at the same time. We have shown, for the first time in an agnostic and model-independent way, that a cuspy DM distribution responsible for the local positron excess is in tension with the gamma-ray data at intermediate Galactic latitudes. We cannot rule out any of the scenarios given all the uncertainties in the modelling. However, there is a preference for a cored DM distribution, which is in agreement with the gamma-ray data, over a cuspy one. Furthermore, and regardless of the actual physical origin of the extra positrons, we found that the contribution from ICS emission is expected to be significant at intermediate latitudes.

All in all, and given all the findings in this work, we are optimistic about our aim of connecting and explaining simultaneously both the positron excess and the whole gamma-ray sky. Extending the energy range and considering other wavelengths will be very helpful for this purpose. Besides this, a more realistic setup combining our studied scenarios might yield more satisfactory results. These possibilities, together with the addition of the missing gamma-ray components, will be explored out in a future work.

Acknowledgments

A SNR contribution to the leptonic gamma-ray emission

As stated in section 4, the π^0 component of the gamma-ray sky comes from the baseline SNR injection. However, this baseline model also contributes to the leptonic gamma-ray emission through its secondary electrons and positrons. The residuals of this baseline model and their contribution to the total gamma-ray emission can be found in figure 7 and figure 8, respectively. The results are similar to those of the PWN scenario, since this profile does not inject many extra e^-e^+ pairs far from the Galactic plane.
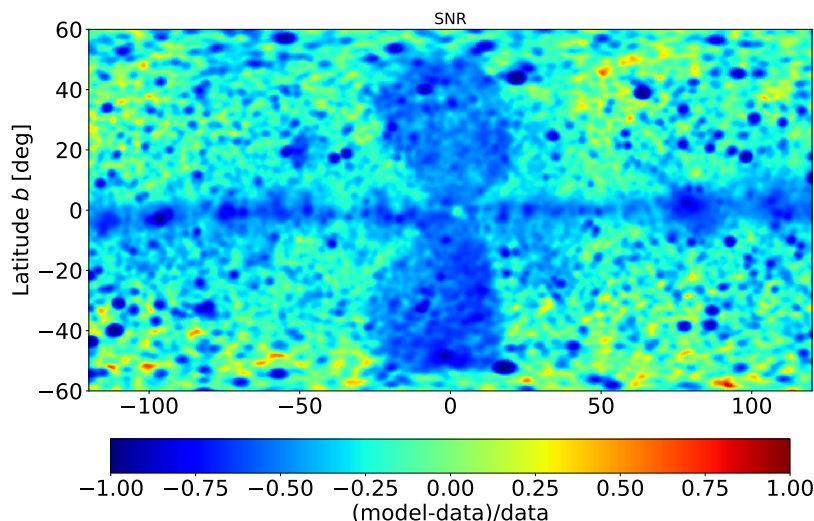

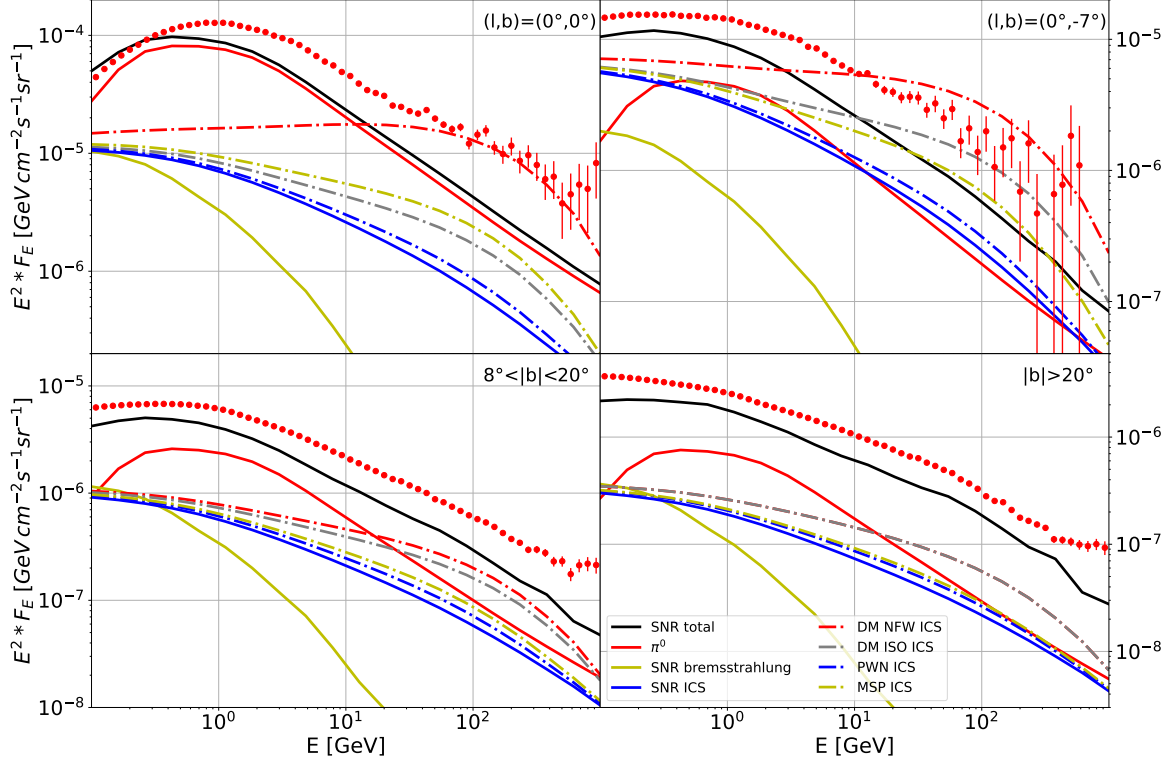**Figure 7.** Residuals of the baseline SNR model.

Figure 8. Gamma-ray spectra of the baseline SNR model, for different Galactic regions (specified on the top right of each panel). Its contribution from secondary electrons and positrons is depicted as solid blue (for ICS) and green (bremsstrahlung). The dash-dotted lines represent the ICS component of the rest of scenarios studied in this paper.

References

[1] P. Blasi, *The Origin of Galactic Cosmic Rays*, *Astron. Astrophys. Rev.* **21** (2013) 70 [`arXiv:1311.7346`] [ɪɴSPIRE].

[2] I.V. Moskalenko and A.W. Strong, *Production and propagation of cosmic ray positrons and electrons*, *Astrophys. J.* **493** (1998) 694 [`astro-ph/9710124`] [ɪɴSPIRE].

[3] N. Prantzos et al., *The 511 keV emission from positron annihilation in the Galaxy*, *Rev. Mod. Phys.* **83** (2011) 1001 [`arXiv:1009.4620`] [ɪɴSPIRE].

[4] A.C. Vincent, P. Martin and J.M. Cline, *Interacting dark matter contribution to the Galactic 511 keV gamma ray emission: constraining the morphology with INTEGRAL/SPI observations*, *JCAP* **04** (2012) 022 [`arXiv:1201.0997`] [ɪɴSPIRE].

[5] P. De la Torre Luque, S. Balaji and P. Carenza, *Multimessenger search for electrophilic feebly interacting particles from supernovae*, *Phys. Rev. D* **109** (2024) 103028 [`arXiv:2307.13731`] [ɪɴSPIRE].

[6] PAMELA collaboration, *An anomalous positron abundance in cosmic rays with energies 1.5–100 GeV*, *Nature* **458** (2009) 607 [`arXiv:0810.4995`] [ɪɴSPIRE].

[7] AMS collaboration, *Electron and Positron Fluxes in Primary Cosmic Rays Measured with the Alpha Magnetic Spectrometer on the International Space Station*, *Phys. Rev. Lett.* **113** (2014) 121102 [ɪɴSPIRE].

[8] FERMI-LAT collaboration, *Cosmic-ray electron-positron spectrum from 7 GeV to 2 TeV with the Fermi Large Area Telescope*, *Phys. Rev. D* **95** (2017) 082007 [arXiv:1704.07195] [INSPIRE].

[9] R. Diesing and D. Caprioli, *Nonsecondary origin of cosmic ray positrons*, *Phys. Rev. D* **101** (2020) 103030 [arXiv:2001.02240] [INSPIRE].

[10] D. Hooper, P. Blasi and P.D. Serpico, *Pulsars as the Sources of High Energy Cosmic Ray Positrons*, *JCAP* **01** (2009) 025 [arXiv:0810.1527] [INSPIRE].

[11] D. Hooper, I. Cholis, T. Linden and K. Fang, *HAWC Observations Strongly Favor Pulsar Interpretations of the Cosmic-Ray Positron Excess*, *Phys. Rev. D* **96** (2017) 103013 [arXiv:1702.08436] [INSPIRE].

[12] I. Cholis, T. Karwal and M. Kamionkowski, *Features in the Spectrum of Cosmic-Ray Positrons from Pulsars*, *Phys. Rev. D* **97** (2018) 123011 [arXiv:1712.00011] [INSPIRE].

[13] M. Di Mauro, S. Manconi and F. Donato, *Detection of a γ-ray halo around Geminga with the Fermi -LAT data and implications for the positron flux*, *Phys. Rev. D* **100** (2019) 123015 [*Erratum ibid.* **104** (2021) 089903] [arXiv:1903.05647] [INSPIRE].

[14] S. Manconi, M. Di Mauro and F. Donato, *Contribution of pulsars to cosmic-ray positrons in light of recent observation of inverse-Compton halos*, *Phys. Rev. D* **102** (2020) 023015 [arXiv:2001.09985] [INSPIRE].

[15] O. Fornieri, D. Gaggero and D. Grasso, *Features in cosmic-ray lepton data unveil the properties of nearby cosmic accelerators*, *JCAP* **02** (2020) 009 [arXiv:1907.03696] [INSPIRE].

[16] C. Evoli, E. Amato, P. Blasi and R. Aloisio, *Galactic factories of cosmic-ray electrons and positrons*, *Phys. Rev. D* **103** (2021) 083010 [arXiv:2010.11955] [INSPIRE].

[17] M. Boudaud et al., *A new look at the cosmic ray positron fraction*, *Astron. Astrophys.* **575** (2015) A67 [arXiv:1410.3799] [INSPIRE].

[18] H.-B. Jin, Y.-L. Wu and Y.-F. Zhou, *Cosmic ray propagation and dark matter in light of the latest AMS-02 data*, *JCAP* **09** (2015) 049 [arXiv:1410.0171] [INSPIRE].

[19] H.-B. Jin, Y.-L. Wu and Y.-F. Zhou, *Astrophysical background and dark matter implication based on latest AMS-02 data*, *Astrophys. J.* **901** (2020) 80 [arXiv:1701.02213] [INSPIRE].

[20] H. Zhan, *Constraining the dark matter interpretation of the positron excess with γ-ray data*, arXiv:2305.01992 [INSPIRE].

[21] L. Goodenough and D. Hooper, *Possible Evidence For Dark Matter Annihilation In The Inner Milky Way From The Fermi Gamma Ray Space Telescope*, arXiv:0910.2998 [INSPIRE].

[22] D. Hooper and L. Goodenough, *Dark Matter Annihilation in The Galactic Center As Seen by the Fermi Gamma Ray Space Telescope*, *Phys. Lett. B* **697** (2011) 412 [arXiv:1010.2752] [INSPIRE].

[23] D. Hooper and T. Linden, *On The Origin Of The Gamma Rays From The Galactic Center*, *Phys. Rev. D* **84** (2011) 123005 [arXiv:1110.0006] [INSPIRE].

[24] A. Boyarsky, D. Malyshev and O. Ruchayskiy, *A comment on the emission from the Galactic Center as seen by the Fermi telescope*, *Phys. Lett. B* **705** (2011) 165 [arXiv:1012.5839] [INSPIRE].

[25] K.N. Abazajian and M. Kaplinghat, *Detection of a Gamma-Ray Source in the Galactic Center Consistent with Extended Emission from Dark Matter Annihilation and Concentrated Astrophysical Emission*, *Phys. Rev. D* **86** (2012) 083511 [*Erratum ibid.* **87** (2013) 129902] [arXiv:1207.6047] [INSPIRE].

[26] C. Gordon and O. Macías, *Dark Matter and Pulsar Model Constraints from Galactic Center Fermi-LAT Gamma Ray Observations*, *Phys. Rev. D* **88** (2013) 083521 [*Erratum ibid.* **89** (2014) 049901] [arXiv:1306.5725] [INSPIRE].

[27] K.N. Abazajian, N. Canac, S. Horiuchi and M. Kaplinghat, *Astrophysical and Dark Matter Interpretations of Extended Gamma-Ray Emission from the Galactic Center*, *Phys. Rev. D* **90** (2014) 023526 [arXiv:1402.4090] [INSPIRE].

[28] F. Calore, I. Cholis, C. McCabe and C. Weniger, *A Tale of Tails: Dark Matter Interpretations of the Fermi GeV Excess in Light of Background Model Systematics*, *Phys. Rev. D* **91** (2015) 063003 [arXiv:1411.4647] [INSPIRE].

[29] F. Calore, I. Cholis and C. Weniger, *Background Model Systematics for the Fermi GeV Excess*, *JCAP* **03** (2015) 038 [arXiv:1409.0042] [INSPIRE].

[30] T. Daylan et al., *The characterization of the gamma-ray signal from the central Milky Way: A case for annihilating dark matter*, *Phys. Dark Univ.* **12** (2016) 1 [arXiv:1402.6703] [INSPIRE].

[31] FERMI-LAT collaboration, *Fermi-LAT Observations of High-Energy γ-Ray Emission Toward the Galactic Center*, *Astrophys. J.* **819** (2016) 44 [arXiv:1511.02938] [INSPIRE].

[32] FERMI-LAT collaboration, *The Fermi Galactic Center GeV Excess and Implications for Dark Matter*, *Astrophys. J.* **840** (2017) 43 [arXiv:1704.03910] [INSPIRE].

[33] M. Di Mauro et al., *Search for γ-ray emission from dark matter particle interactions from Andromeda and Triangulum Galaxies with the Fermi Large Area Telescope*, *Phys. Rev. D* **99** (2019) 123027 [arXiv:1904.10977] [INSPIRE].

[34] R. Bartels, S. Krishnamurthy and C. Weniger, *Strong support for the millisecond pulsar origin of the Galactic center GeV excess*, *Phys. Rev. Lett.* **116** (2016) 051102 [arXiv:1506.05104] [INSPIRE].

[35] R. Bartels, F. Calore, E. Storm and C. Weniger, *Galactic binaries can explain the Fermi Galactic centre excess and 511 keV emission*, *Mon. Not. Roy. Astron. Soc.* **480** (2018) 3826 [arXiv:1803.04370] [INSPIRE].

[36] C. Venter et al., *Cosmic-ray positrons from millisecond pulsars*, *Astrophys. J.* **807** (2015) 130 [arXiv:1506.01211] [INSPIRE].

[37] M. Linares and M. Kachelriess, *Cosmic ray positrons from compact binary millisecond pulsars*, *JCAP* **02** (2021) 030 [arXiv:2010.02844] [INSPIRE].

[38] FERMI-LAT collaboration, *Development of the Model of Galactic Interstellar Emission for Standard Point-Source Analysis of Fermi Large Area Telescope Data*, *Astrophys. J. Suppl.* **223** (2016) 26 [arXiv:1602.07246] [INSPIRE].

[39] E. Storm, C. Weniger and F. Calore, *SkyFACT: High-dimensional modeling of gamma-ray emission with adaptive templates and penalized likelihoods*, *JCAP* **08** (2017) 022 [arXiv:1705.04065] [INSPIRE].

[40] M. Pohl, O. Macías, P. Coleman and C. Gordon, *Assessing the Impact of Hydrogen Absorption on the Characteristics of the Galactic Center Excess*, *Astrophys. J.* **929** (2022) 136 [arXiv:2203.11626] [INSPIRE].

[41] FERMI-LAT collaboration, *Fermi-LAT Observations of the Diffuse γ-Ray Emission: Implications for Cosmic Rays and the Interstellar Medium*, *Astrophys. J.* **750** (2012) 3 [arXiv:1202.4039] [INSPIRE].

[42] E. Orlando, *Imprints of Cosmic Rays in Multifrequency Observations of the Interstellar Emission*, *Mon. Not. Roy. Astron. Soc.* **475** (2018) 2724 [`arXiv:1712.07127`] [ɪɴSPIRE].

[43] I. Cholis, Y.-M. Zhong, S.D. McDermott and J.P. Surdutovich, *Return of the templates: Revisiting the Galactic Center excess with multimessenger observations*, *Phys. Rev. D* **105** (2022) 103023 [`arXiv:2112.09706`] [ɪɴSPIRE].

[44] J. Thaler, R. Kissmann and O. Reimer, *Cosmic-ray propagation under consideration of a spatially resolved source distribution*, *Astropart. Phys.* **144** (2023) 102776 [`arXiv:2209.02295`] [ɪɴSPIRE].

[45] P.D.T. Luque et al., *Galactic diffuse gamma rays meet the PeV frontier*, *Astron. Astrophys.* **672** (2023) A58 [`arXiv:2203.15759`] [ɪɴSPIRE].

[46] R. Trotta et al., *Constraints on cosmic-ray propagation models from a global Bayesian analysis*, *Astrophys. J.* **729** (2011) 106 [`arXiv:1011.0037`] [ɪɴSPIRE].

[47] M. Korsmeier and A. Cuoco, *Galactic cosmic-ray propagation in the light of AMS-02: Analysis of protons, helium, and antiprotons*, *Phys. Rev. D* **94** (2016) 123019 [`arXiv:1607.06093`] [ɪɴSPIRE].

[48] C. Evoli, R. Aloisio and P. Blasi, *Galactic cosmic rays after the AMS-02 observations*, *Phys. Rev. D* **99** (2019) 103023 [`arXiv:1904.10220`] [ɪɴSPIRE].

[49] C. Evoli, G. Morlino, P. Blasi and R. Aloisio, *AMS-02 beryllium data and its implication for cosmic ray transport*, *Phys. Rev. D* **101** (2020) 023013 [`arXiv:1910.04113`] [ɪɴSPIRE].

[50] P.D.L.T. Luque et al., *Markov chain Monte Carlo analyses of the flux ratios of B, Be and Li with the DRAGON2 code*, *JCAP* **07** (2021) 010 [`arXiv:2102.13238`] [ɪɴSPIRE].

[51] V.L. Ginzburg and S.I. Syrovatskii, *The Origin of Cosmic Rays*, Pergamon (1964) [`DOI:10.1016/C2013-0-05547-8`].

[52] V.S. Berezinskii, S.V. Bulanov, V.A. Dogiel and V.S. Ptuskin, *Astrophysics of cosmic rays*, V.L. Ginzburg ed., North-Holland (1990) [ɪɴSPIRE].

[53] C. Evoli et al., *Cosmic-ray propagation with DRAGON2: I. numerical solver and astrophysical ingredients*, *JCAP* **02** (2017) 015 [`arXiv:1607.07886`] [ɪɴSPIRE].

[54] O. Fornieri et al., *Diffusive origin for the cosmic-ray spectral hardening reveals signatures of a nearby source in the leptons and protons data*, *Phys. Rev. D* **104** (2021) 103013 [`arXiv:2007.15321`] [ɪɴSPIRE].

[55] G. Di Bernardo et al., *Cosmic Ray Electrons, Positrons and the Synchrotron emission of the Galaxy: consistent analysis and implications*, *JCAP* **03** (2013) 036 [`arXiv:1210.4546`] [ɪɴSPIRE].

[56] AMS collaboration, *Towards Understanding the Origin of Cosmic-Ray Positrons*, *Phys. Rev. Lett.* **122** (2019) 041102 [ɪɴSPIRE].

[57] K.M. Ferrière, *The interstellar environment of our galaxy*, *Rev. Mod. Phys.* **73** (2001) 1031 [`astro-ph/0106359`] [ɪɴSPIRE].

[58] D.R. Lorimer et al., *The Parkes multibeam pulsar survey: VI. Discovery and timing of 142 pulsars and a Galactic population analysis*, *Mon. Not. Roy. Astron. Soc.* **372** (2006) 777 [`astro-ph/0607640`] [ɪɴSPIRE].

[59] P.J. McMillan, *The mass distribution and gravitational potential of the Milky Way*, *Mon. Not. Roy. Astron. Soc.* **465** (2016) 76 [`arXiv:1608.00971`] [ɪɴSPIRE].

[60] R.A. Flores and J.R. Primack, *Observational and theoretical constraints on singular dark matter halos*, *Astrophys. J. Lett.* **427** (1994) L1 [`astro-ph/9402004`] [ɪɴSPIRE].

[61] B. Moore, *Evidence against dissipationless dark matter from observations of galaxy haloes*, *Nature* **370** (1994) 629 [ɪɴSPIRE].

[62] A. Di Cintio et al., *The dependence of dark matter profiles on the stellar-to-halo mass ratio: a prediction for cusps versus cores*, *Mon. Not. Roy. Astron. Soc.* **437** (2014) 415 [`arXiv:1306.0898`] [ɪɴSPIRE].

[63] M. Benito, A. Cuoco and F. Iocco, *Handling the Uncertainties in the Galactic Dark Matter Distribution for Particle Dark Matter Searches*, *JCAP* **03** (2019) 033 [`arXiv:1901.02460`] [ɪɴSPIRE].

[64] J.F. Navarro, C.S. Frenk and S.D.M. White, *The structure of cold dark matter halos*, *Astrophys. J.* **462** (1996) 563 [`astro-ph/9508025`] [ɪɴSPIRE].

[65] K.G. Begeman, A.H. Broeils and R.H. Sanders, *Extended rotation curves of spiral galaxies: Dark haloes and modified dynamics*, *Mon. Not. Roy. Astron. Soc.* **249** (1991) 523 [ɪɴSPIRE].

[66] M. Pato, F. Iocco and G. Bertone, *Dynamical constraints on the dark matter distribution in the Milky Way*, *JCAP* **12** (2015) 001 [`arXiv:1504.06324`] [ɪɴSPIRE].

[67] G. Bertone, D. Hooper and J. Silk, *Particle dark matter: Evidence, candidates and constraints*, *Phys. Rept.* **405** (2005) 279 [`hep-ph/0404175`] [ɪɴSPIRE].

[68] M.S. Pshirkov, P.G. Tinyakov, P.P. Kronberg and K.J. Newton-McGee, *Deriving global structure of the Galactic Magnetic Field from Faraday Rotation Measures of extragalactic sources*, *Astrophys. J.* **738** (2011) 192 [`arXiv:1103.0814`] [ɪɴSPIRE].

[69] A.W. Strong, E. Orlando and T.R. Jaffe, *The interstellar cosmic-ray electron spectrum from synchrotron radiation and direct measurements*, *Astron. Astrophys.* **534** (2011) A54 [`arXiv:1108.4822`] [ɪɴSPIRE].

[70] E. Orlando and A. Strong, *Galactic synchrotron emission with cosmic ray propagation models*, *Mon. Not. Roy. Astron. Soc.* **436** (2013) 2127 [`arXiv:1309.2947`] [ɪɴSPIRE].

[71] A. Dundovic, C. Evoli, D. Gaggero and D. Grasso, *Simulating the Galactic multi-messenger emissions with HERMES*, *Astron. Astrophys.* **653** (2021) A18 [`arXiv:2105.13165`] [ɪɴSPIRE].

[72] HI4PI collaboration et al., *HI4PI: A full-sky H I survey based on EBHIS and GASS*, *Astron. Astrophys.* **594** (2016) A116 [`arXiv:1610.06175`].

[73] T.M. Dame, D. Hartmann and P. Thaddeus, *The Milky Way in molecular clouds: A new complete co survey*, *Astrophys. J.* **547** (2001) 792 [`astro-ph/0009217`] [ɪɴSPIRE].

[74] A.W. Strong and J.R. Mattox, *Gradient model analysis of EGRET diffuse Galactic γ-ray emission*, *Astron. Astrophys.* **308** (1996) L21.

[75] C. Evoli et al., *Cosmic-ray propagation with DRAGON2: II. Nuclear interactions with the interstellar gas*, *JCAP* **07** (2018) 006 [`arXiv:1711.09616`] [ɪɴSPIRE].

[76] T. Kamae et al., *Parameterization of γ, $e^{\pm}$ and Neutrino Spectra Produced by p-p Interaction in Astronomical Environment*, *Astrophys. J.* **647** (2006) 692 [*Erratum ibid.* **662** (2007) 779] [`astro-ph/0605581`] [ɪɴSPIRE].

[77] AMS collaboration, *The Alpha Magnetic Spectrometer (AMS) on the international space station: Part II — Results from the first seven years*, *Phys. Rept.* **894** (2021) 1 [ɪɴSPIRE].

[78] H.E.S.S. collaboration, *The energy spectrum of cosmic-ray electrons at TeV energies*, *Phys. Rev. Lett.* **101** (2008) 261104 [`arXiv:0811.3894`] [ɪɴSPIRE].

[79] A.C. Cummings et al., *Galactic Cosmic Rays in the Local Interstellar Medium: Voyager 1 Observations and Model Results*, *Astrophys. J.* **831** (2016) 18 [InSPIRE].

[80] I.G. Usoskin, K. Alanko-Huotari, G.A. Kovaltsov and K. Mursula, *Heliospheric modulation of cosmic rays: Monthly reconstruction for 1951-2004*, *J. Geophys. Res.* **110** (2005) A12108.

[81] I.G. Usoskin, G.A. Bazilevskaya and G.A. Kovaltsov, *Solar modulation parameter for cosmic rays since 1936 reconstructed from ground-based neutron monitors and ionization chambers*, *J. Geophys. Res.* **116** (2011) A02104.

[82] P. De la Torre Luque, F. Loparco and M.N. Mazziotta, *The FLUKA cross sections for cosmic-ray leptons and uncertainties on current positron predictions*, *JCAP* **10** (2023) 011 [arXiv:2305.02958] [InSPIRE].

[83] S. Koldobskiy et al., *Energy spectra of secondaries in proton-proton interactions*, *Phys. Rev. D* **104** (2021) 123027 [arXiv:2110.00496] [InSPIRE].

[84] L. Orusa, M.D. Mauro, F. Donato and M. Korsmeier, *New determination of the production cross section for secondary positrons and electrons in the Galaxy*, *Phys. Rev. D* **105** (2022) 123021 [arXiv:2203.13143].

[85] E. Silver and E. Orlando, *Testing Cosmic-Ray Propagation Scenarios with AMS-02 and Voyager Data*, *Astrophys. J.* **963** (2024) 111 [arXiv:2401.06242] [InSPIRE].

[86] R. Aloisio and P. Blasi, *Propagation of galactic cosmic rays in the presence of self-generated turbulence*, *JCAP* **2013** (2013) 001 [arXiv:1306.2018].

[87] M.J. Boschini et al., *Inference of the Local Interstellar Spectra of Cosmic-Ray Nuclei $Z \leq 28$ with the GalProp-HelMod Framework*, *Astrophys. J. Suppl.* **250** (2020) 27 [arXiv:2006.01337] [InSPIRE].

[88] P. Blasi and E. Amato, *Diffusive propagation of cosmic rays from supernova remnants in the Galaxy. I: spectrum and chemical composition*, *JCAP* **01** (2012) 010 [arXiv:1105.4521] [InSPIRE].

[89] P. Reichherzer et al., *Regimes of cosmic-ray diffusion in Galactic turbulence*, *SN Appl. Sci.* **4** (2022) 15 [arXiv:2104.13093] [InSPIRE].

[90] M. Di Mauro et al., *Novel prediction for secondary positrons and electrons in the Galaxy*, *Phys. Rev. D* **108** (2023) 063024 [arXiv:2304.01261] [InSPIRE].

[91] S.-Q. Xi et al., *GeV observations of the extended pulsar wind nebulae constrain the pulsar interpretations of the cosmic-ray positron excess*, *Astrophys. J.* **878** (2019) 104 [arXiv:1810.10928] [InSPIRE].

[92] J. Petrović, P.D. Serpico and G. Zaharijas, *Millisecond pulsars and the Galactic Center gamma-ray excess: the importance of luminosity function and secondary emission*, *JCAP* **02** (2015) 023 [arXiv:1411.2980] [InSPIRE].

[93] O. Macías et al., *Cherenkov Telescope Array sensitivity to the putative millisecond pulsar population responsible for the Galactic Centre excess*, *Mon. Not. Roy. Astron. Soc.* **506** (2021) 1741 [arXiv:2102.05648] [InSPIRE].

[94] FERMI-LAT collaboration, *The spectrum of isotropic diffuse gamma-ray emission between 100 MeV and 820 GeV*, *Astrophys. J.* **799** (2015) 86 [arXiv:1410.3696] [InSPIRE].

[95] M. Fornasa and M.A. Sánchez-Conde, *The nature of the Diffuse Gamma-Ray Background*, *Phys. Rept.* **598** (2015) 1 [arXiv:1502.02866] [InSPIRE].

[96] M. Pohl, P. Englmaier and N. Bissantz, *3D Distribution of Molecular Gas in the Barred Milky Way*, *Astrophys. J.* **677** (2008) 283 [`arXiv:0712.4264`] [INSPIRE].

[97] M. Su, T.R. Slatyer and D.P. Finkbeiner, *Giant Gamma-ray Bubbles from Fermi-LAT: AGN Activity or Bipolar Galactic Wind?*, *Astrophys. J.* **724** (2010) 1044 [`arXiv:1005.5480`] [INSPIRE].

[98] FERMI-LAT collaboration, *The Spectrum and Morphology of the Fermi Bubbles*, *Astrophys. J.* **793** (2014) 64 [`arXiv:1407.7905`] [INSPIRE].

[99] M. Tavakoli, I. Cholis, C. Evoli and P. Ullio, *Constraints on Dark Matter Annihilations from Diffuse Gamma-Ray Emission in the Galaxy*, *JCAP* **01** (2014) 017 [`arXiv:1308.4135`] [INSPIRE].

[100] M. Cirelli, *Status of Indirect (and Direct) Dark Matter searches*, *PoS* **ICRC2015** (2016) 014 [`arXiv:1511.02031`] [INSPIRE].

[101] P. Martin, L. Tibaldo, A. Marcowith and S. Abdollahi, *Population synthesis of pulsar wind nebulae and pulsar halos in the Milky Way — Predicted contributions to the very-high-energy sky*, *Astron. Astrophys.* **666** (2022) A7 [`arXiv:2207.11178`] [INSPIRE].

[102] R. Catena and P. Ullio, *A novel determination of the local dark matter density*, *JCAP* **08** (2010) 004 [`arXiv:0907.0018`] [INSPIRE].

[103] M. Wechakama and Y. Ascasibar, *Pressure from dark matter annihilation and the rotation curve of spiral galaxies*, *Mon. Not. Roy. Astron. Soc.* **413** (2011) 1991 [`arXiv:1007.3179`] [INSPIRE].

[104] M. Wechakama and Y. Ascasibar, *Multimessenger constraints on dark matter annihilation into electron-positron pairs*, *Mon. Not. Roy. Astron. Soc.* **439** (2014) 566 [`arXiv:1212.2583`] [INSPIRE].

[105] H.E.S.S. collaboration, *Search for Dark Matter Annihilation Signals in the H.E.S.S. Inner Galaxy Survey*, *Phys. Rev. Lett.* **129** (2022) 111101 [`arXiv:2207.10471`] [INSPIRE].

[106] I. Krommydas and I. Cholis, *Revisiting GeV-scale annihilating dark matter with the AMS-02 positron fraction*, *Phys. Rev. D* **107** (2023) 023003 [`arXiv:2210.04903`] [INSPIRE].

[107] E. Orlando, *Implications on Spatial Models of Interstellar Gamma-Ray Inverse-Compton Emission from Synchrotron Emission Studies in Radio and Microwaves*, *Phys. Rev. D* **99** (2019) 043007 [`arXiv:1901.08604`] [INSPIRE].

[108] R. Barak, K. Belotsky and E. Shlepkina, *Proposition of FSR Photon Suppression Employing a Two-Positron Decay Dark Matter Model to Explain Positron Anomaly in Cosmic Rays*, *Universe* **9** (2023) 370 [`arXiv:2310.06859`] [INSPIRE].